

RESEARCH

Open Access



Synthesis, structural determination and antimicrobial evaluation of two novel Co^{II} and Zn^{II} halogenometallates as efficient catalysts for the acetalization reaction of aldehydes

Assila Maatar Ben Salah¹, Lilia Belghith Fendri², Thierry Bataille³, Raquel P. Herrera⁴ and Houcine Naili^{1*}

Abstract

Background: Complexes of imidazole derivatives with transition metal ions have attracted much attention because of their biological and pharmacological activities, such as antimicrobial, antifungal, antiallergic, antitumoural and antimetastatic properties. In addition, imidazoles occupy an important place owing to their meaningful catalytic activity in several processes, such as in hydroamination, hydrosilylation, Heck reaction and Henry reaction. In this work, we describe the crystallization of two halogenometallate based on 2-methylimidazole. Their IR, thermal analysis, catalytic properties and antibacterial activities have also been investigated.

Results: Two new isostructural organic-inorganic hybrid materials, based on 2-methyl-1*H*-imidazole, **1** and **2**, were synthesized and fully structurally characterized. The analysis of their crystal packing reveals non-covalent interactions, including C/N–H...Cl hydrogen bonds and $\pi\cdots\pi$ stacking interactions, to be the main factor governing the supramolecular assembly of the crystalline complexes. The thermal decomposition of the complexes is a mono-stage process, confirmed by the three-dimensional representation of the powder diffraction patterns (TDXD). The catalytic structure exhibited promising activity using MeOH as solvent and as the unique source of acetalization. Moreover, the antimicrobial results suggested that metal-complexes exhibit significant antimicrobial activity.

Conclusion: This study highlights again the structural and the biological diversities within the field of inorganic-organic hybrids.

Keywords: Halogenometallate, X-ray diffraction, Thermal analysis, Antibacterial activities, Hydrogen bonds, Supramolecular architecture, Catalysis

Introduction

The chemistry of organic-inorganic hybrid materials constitutes one of the most flourishing areas of research in solid-state chemistry [1–3]. These hybrids are of interest because of their wide range of technologically advantageous properties, astounding compositional breadth,

and exceptional diversity of structure. Thus, as a result of structural integration of organic cations and inorganic counterparts, magnetic [4–6], optical [7, 8], metallic conductivity [9] and catalytic [10, 11] properties have arisen in this class of chemical hybrid systems. Moreover, these materials may be used as model compounds for biological applications [12].

In our research, we particularly focus our attention on the preparation and the development of reactive transition metal complexes containing imidazole function for new, more selective or more widely catalytic

*Correspondence: houcine_naili@yahoo.com

¹ Laboratoire Physicochimie de l'Etat Solide, Département de Chimie, Faculté des Sciences de Sfax, Université de Sfax, BP 1171, 3000 Sfax, Tunisia

Full list of author information is available at the end of the article

and biological applications. Various metal complexes, especially these containing imidazole groups, occupy an important place owing to their meaningful catalytic activity in several processes, such as in hydroamination [13–16], hydrosilylation [17, 18] Heck reaction [19–23] and Henry reaction [24]. In addition, imidazoles play an important role in medicinal chemistry, because many of its derivatives have demonstrated significant biological activity. For example, in many metalloenzymes the imidazole rings of histidines play a pivotal role in metal-enzyme coordination. In consequence, the metal complexes of imidazoles have been widely used as model compounds of metalloenzymes [25–29]. It is well known that metal ions present in complexes accelerate the drug action and the efficacy of the organic therapeutic agents [30]. The pharmacological efficiencies of metal complexes depend on the nature of the metal ions and the ligands [31]. It is declared in the literature that different ligands and different complexes synthesized from same ligands with different metal ions possess different biological properties [30, 32, 33]. So, there is an increasing requirement for the discovery of new hybrid compounds having antimicrobial activities. However, this work has been quite selective. In this study, as an extension of our efforts into the development of new metal based antimicrobial complexes with 2-methylimidazole [34], we describe the crystallization of bis(2-methyl-1*H*-imidazolium)tetrachlorocobaltate(II) ($C_4H_7N_2$)₂[CoCl₄] (**1**) and bis(2-methyl-1*H*-imidazolium)tetrachlorozincate(II) ($C_4H_7N_2$)₂[ZnCl₄] (**2**), along with their crystal packing and crystal supramolecularity analyses. Their IR, thermal analysis, catalytic properties and antibacterial activities have also been investigated.

Experimental section

Materials

All the employed chemicals [Cobalt(II) chloride hexahydrate (CoCl₂·6H₂O), Zinc(II) chloride (ZnCl₂), Hydrochloric acid (HCl; 37%) and 2-methyl-1*H*-imidazole ($C_4H_6N_2$)] were commercial products (Sigma-Aldrich), which were used without further purification. All culture media and standard antibiotic were purchased from Bio-Rad laboratories, France).

Synthesis

The two new compounds ($C_4H_7N_2$)₂[CoCl₄] (**1**) and ($C_4H_7N_2$)₂[ZnCl₄] (**2**) were obtained by slow evaporation, at room temperature. 2-Methyl-1*H*-imidazole (2mim) was dissolved with either CoCl₂·6H₂O or ZnCl₂ in 10 mL of distilled water and hydrochloric acid HCl (pH ≈ 2.5) with the metal/amine molar ratio of 1:2. The clear solutions were stirred for 10 min until the complete dissolution and allowed to stand at room temperature. Transparent block crystals with the specific color of the

metal appeared after few days. Then, the products were filtered off and washed with a small amount of distilled water before being dried in ambient air. Otherwise, they are also stable for a long-time in normal conditions of temperature and humidity.

Single-crystal data collection and structure determination

Small crystals of the two compounds **1** and **2** were glued to a glass fiber mounted on a four-circle Nonius KappaCCD area-detector diffractometer with graphite monochromatized Mo K α radiation, using an Oxford Cryosystems cooler. Data collection, absorption corrections frame scaling and unit cell parameters refinements were carried out with CrysAlisCCD and CrysAlisRED [35]. The structures analyses were carried out with the monoclinic symmetry, space groups C2/c, according to the automated search for space group available in Wingx [36]. Structures of **1** and **2** were solved with direct methods using SHELXS-97 [37] and refined by a full-matrix least squares technique with SHELXL-97 [37] with anisotropic thermal parameters for all non H-atoms. H atoms bonded to C and N atoms were positioned geometrically and allowed to ride on their parent atoms, with C–H = 0.95 Å and N–H = 0.88 Å. The drawings were made with DIAMOND program [38]. The main crystallographic data and refinement parameters are presented in Table 1.

Infrared spectroscopy

All IR measurements were performed using a Perkin Elmer 1600FT spectrometer. Samples were dispersed with spectroscopic KBr and pressed into a pellet. Scans were run over the range 400–4000 cm⁻¹.

Thermal analyses

TGA–DTA measurements of **1** and **2** were performed on raw powders with a TGA/DTA ‘SETSYS Evolution’ (Pt crucibles, Al₂O₃ as a reference) under air flow (100 mL/min). The thermograms were collected on 9 mg samples in the temperature range from 25 to 650 °C (heating rate of 5 °C/min).

Powder X-ray diffraction

The variable-temperature X-ray powder diffraction (VT-XRPD) for **1** and **2** was performed with a PANalytical Empyrean powder diffractometer using CuK α radiation ($\lambda K\alpha_1 = 1.5406$ Å, $\lambda K\alpha_2 = 1.5444$ Å) selected with the Bragg–Brentano HD[®] device (flat multilayer X-ray mirror) from PANalytical and equipped with an Anton Paar HTK1200N high-temperature oven camera. Powder X-ray diffraction was used to support the structure determination and to identify the crystalline phases of **1** and **2**. The thermal decompositions were carried out in flowing air from 20 to 670 °C. Patterns were collected every 7 °C, with a heating rate of 7 °C h⁻¹ between steps.

Table 1 Crystal data and structure refinement details for (C₄H₇N₂)₂[CoCl₄] (1) and (C₄H₇N₂)₂[ZnCl₄] (2)

Compound	(1)	(2)
Chemical formula	(C ₄ H ₇ N ₂) ₂ [CoCl ₄]	(C ₄ H ₇ N ₂) ₂ [ZnCl ₄]
Compound weight	366.96	373.40
Temperature (K)	100 (2)	100 (10)
Crystal system	Monoclinic	Monoclinic
Space group	C2/c	C2/c
a (Å)	26.9330 (17)	26.871 (8)
b (Å)	7.8842 (2)	7.9031 (18)
c (Å)	15.0925 (5)	15.077 (5)
β (°)	111.001 (5)	111.23 (5)
V (Å ³)	2991.9 (2)	2984.5 (15)
Z	8	8
ρ _{cal} (g cm ⁻³)	1.629	1.662
Crystal dimension, mm ³	0.45 × 0.37 × 0.13	0.50 × 0.42 × 0.12
Habit-colour	Block, blue	Block, transparent
μ (mm ⁻¹)	1.85	2.35
θ range (deg)	θ _{min} = 2.7, θ _{max} = 30.7	θ _{min} = 2.7, θ _{max} = 30.7
Index ranges	- 26 ≤ h ≤ 38 - 10 ≤ k ≤ 10 - 21 ≤ l ≤ 21	- 38 ≤ h ≤ 29 - 9 ≤ k ≤ 11 - 21 ≤ l ≤ 21
Unique data	4253	4197
Observed data [I > 2σ(I)]	3254	3731
F(000)	1480	1504
R ₁	0.053	0.050
wR ₂	0.132	0.121
Goof	1.012	1.17
No. param	156	157
Transmission factors	T _{min} = 0.334; T _{max} = 0.804	T _{min} = 0.387; T _{max} = 0.766
Largest difference map hole	Δρ _{min} = - 1.11, Δρ _{max} = 1.44	Δρ _{min} = - 0.63, Δρ _{max} = 2.36

Catalytic studies

Complex **1** (4.7 mg, 0.01292 mmol) or **2** (4.8 mg, 0.01292 mmol) and aldehydes **3a–i** (0.323 mmol) were dissolved in MeOH (0.25 mL) in a test tube. The resulting mixture was stirred at 40 °C during 24 h. The reactions were monitored by thin-layer chromatography. The yield of the reaction is given by ¹H NMR.

Antimicrobial activity

Antimicrobial activity was assayed against three species of Gram negative bacteria [*Salmonella typhimurium* (ATCC 19430), *Pseudomonas aeruginosa* (ATCC 27853), *Klebsiella pneumonia* (ATCC 13883) and five species of Gram positive bacteria (*Enterococcus faecalis* (ATCC 9763), *Bacillus thuringiensis* (ATCC 10792), *Staphylococcus aureus* (ATCC 25923), *Micrococcus luteus* (ATCC 4698) and *listeria*]. All microorganisms were stocked in appropriate conditions and regenerated twice before using.

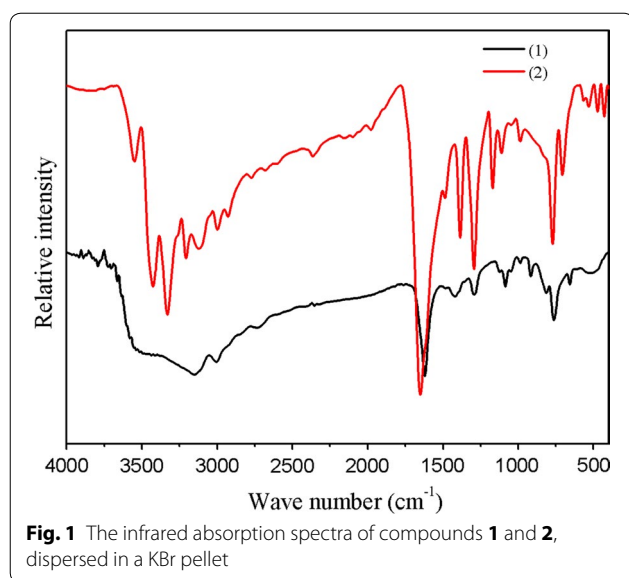
Antimicrobial activity assays were performed according to the method described by Berghe and Vlietinck [39].

Steril enutrient agar medium was prepared and distributed into Petriplates of 90 mm diameter. A suspension of the previously prepared test microorganism (0.1 mL of 10⁶ UFCmL⁻¹) was spread over the surface of agar plates (LB medium for bacteria). Then, bores (3 mm depth, 5 mm diameter) were made using a sterile borer and loaded with a concentration of 5 mg/mL of all samples. Before incubation, all petri dishes were kept in the refrigerator for 2 h to enable pre-diffusion of the substances into the agar. After that, they were incubated at 37 °C for 24 h. Ampicillin was used as positive reference. The diameters of the inhibition zones were measured using a ruler, with an accuracy of 0.5 mm. Each inhibition zone diameter was measured three times (in two different plates) and the results were expressed as an average of the radius of the inhibition zone in mm.

Results and discussion

Infrared spectra

The IR active bands of the 2-mim ring as well as the stretching vibrations of the N–H bond could be identified



in the IR spectra of both compounds (Fig. 1). Indeed, it is known that the narrow bands at 3147.3 and 3120.9 cm^{-1} , for **1** and **2** respectively, correspond to the $\nu_{\text{C-H}}$ stretching modes of the 2-mim ring [40]. Moreover the stretching vibration $\nu(\text{NH})$ has been identified at 2724 and 3752 cm^{-1} , for **1** and **2**, respectively. This agrees well with the structural study which proved the protonation of the 2-mim cation. The bands located in the region 1400–1650 cm^{-1} are assignable to C–C and C–N stretching

vibration of 2-mim ring. The $\nu_{\text{C=N}}$ mode can be found at 1438 and 1492 cm^{-1} for **1** and **2**, respectively. Additionally, the vibrational bands from 1002 to 1438 cm^{-1} can be assigned to the ring stretching frequency of the 2-mim cation (ν_{ring}) [41]. Finally, the bands remaining in the 686–859 cm^{-1} region can be associated with the deformations of the imidazole ring.

Crystal structure

Compounds **1** and **2** are isostructural, confirmed by their single crystal structural analyses (Table 1). Compound **1** was taken as an example to understand the structural details. Complex **1** crystallizes in the monoclinic centrosymmetric space group $C2/c$ and its basic structure unit consists of one $[\text{CoCl}_4]^{2-}$ ion and two crystallographically inequivalent 2-mim cations, as shown in Fig. 2.

The Co(II) ion is tetrahedrally bound by four chlorine atoms, with Co–Cl bond distances ranging from 2.246(9) to 2.287(9) Å and Cl–Co–Cl bond angles between 106.45(4)° and 111.87(3)°, which are slightly deviated from the ideal value of 109.28° (Table 2). Therefore, the coordination geometry around the Co^{II} ion can be described as a slightly irregular tetrahedron. Cobalt atoms are stacked one over the other along the three crystallographic axes and are isolated from each other with a shortest distance $\text{Co}\cdots\text{Co} = 7.330(4)$ Å which is more than the sum of the van der Waals radii of the cobalt ions tetrahedrally coordinated (4 Å). Hence, there

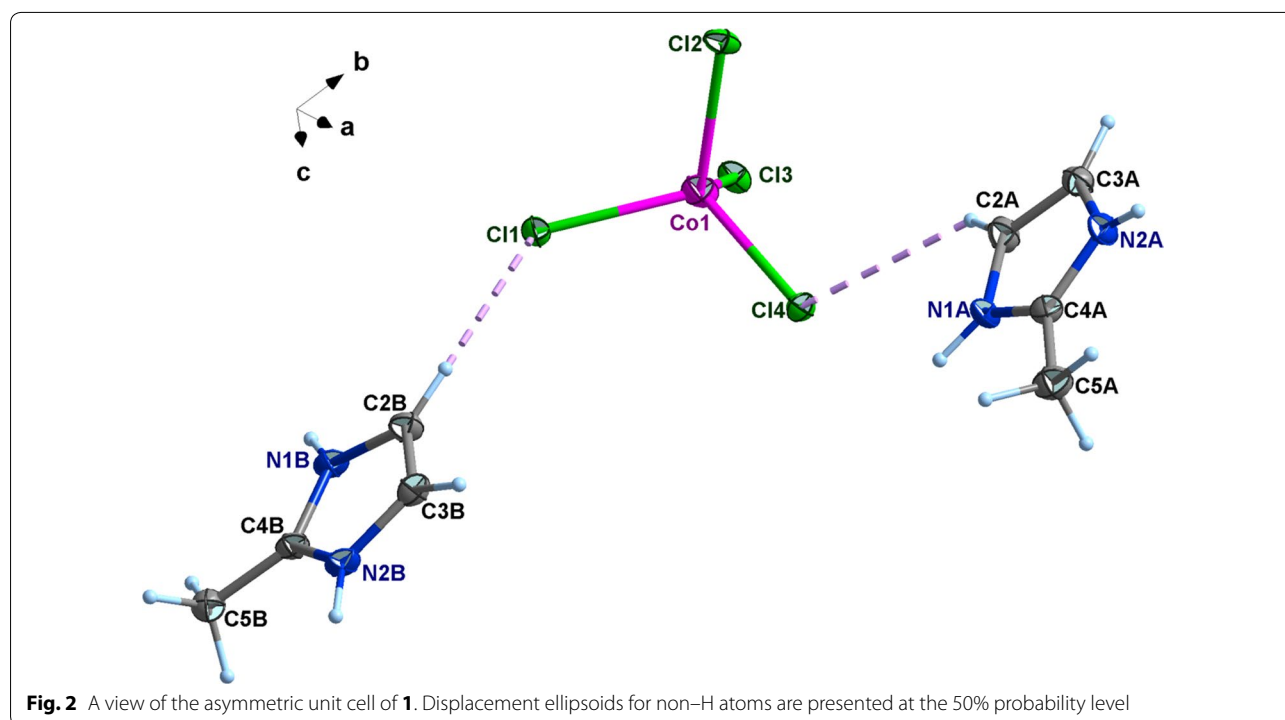


Table 2 Selected bond distances (Å) and angles (°) for 1 and 2

Within the mineral moiety		Within the organic moiety	
$(C_4H_7N_2)_2[CoCl_4]$ (1)			
Co1–Cl1	2.2741 (9)	N1A–C4A	1.325 (5)
Co1–Cl2	2.2767(10)	N1A–C2A	1.380 (5)
Co1–Cl3	2.2870 (9)	N2A–C4A	1.327 (5)
Co1–Cl4	2.2464 (9)	N2A–C3A	1.372 (5)
Cl2–Co1–Cl1	106.45 (4)	N1B–C4B	1.331 (4)
Cl3–Co1–Cl1	108.69 (3)	N1B–C2B	1.374 (5)
Cl3–Co1–Cl2	110.55 (3)	N2B–C4B	1.331(4)
Cl3–Co1–Cl4	109.09 (4)	N2B–C3B	1.370 (5)
Cl2–Co1–Cl4	110.16 (4)	C2A–C3A	1.345(5)
Cl1–Co1–Cl4	111.87 (3)	C4A–C5A	1.479 (6)
		C2B–C3B	1.348 (5)
		C4B–C5B	1.478 (5)
		C4A–N1A–C2A	110.0 (3)
		C4A–N2A–C3A	110.1 (3)
		C4B–N2B–C3B	110.2 (3)
		C4A–N2A–C3A	110.1 (3)
		C3B–C2B–N1B	106.5 (3)
		C3A–C2A–N1A	106.3 (3)
		C2B–C3B–N2B	106.7 (3)
		C2A–C3A–N2A	106.8 (3)
		N1A–C4A–N2A	106.8 (3)
		N1A–C4A–C5A	126.5 (4)
		N2A–C4A–C5A	126.7 (4)
		N1B–C4B–N2B	106.5 (3)
		N1B–C4B–C5B	126.8 (3)
		N2B–C4B–C5B	126.6 (3)
$(C_4H_7N_2)_2[ZnCl_4]$ (2)			
Zn–Cl1	2.2780 (11)	N1A–C2A	1.325 (5)
Zn–Cl2	2.2779 (13)	N1A–C3A	1.381 (6)
Zn–Cl3	2.2392 (16)	N2A–C2A	1.335 (5)
Zn–Cl4	2.2945 (13)	N2A–C4A	1.386 (6)
Cl2–Zn–Cl1	106.45 (5)	C1A–C2A	1.438 (6)
Cl3–Zn–Cl1	112.11 (4)	C3A–C4A	1.347 (6)
Cl3–Zn–Cl2	110.49 (5)	N1B–C2B	1.336 (5)
Cl3–Zn–Cl4	109.43 (5)	N1B–C3B	1.372 (6)
Cl2–Zn–Cl4	109.98 (4)	N2B–C2B	1.332 (5)
Cl1–Zn–Cl4	108.31 (4)	N2B–C4B	1.380 (6)
		C1B–C2B	1.471 (6)
		C3B–C4B	1.348 (6)
		C3A–C4A–N2A	106.7 (4)
		C2A–N2A–C4A	109.8 (3)
		N1A–C2A–N2A	106.8 (4)
		N1A–C2A–C1A	126.6 (4)
		N2A–C2A–C1A	126.6 (4)
		C4A–C3A–N1A	106.7 (4)
		C2B–N1B–C3B	110.3 (4)
		C2B–N2B–C4B	110.3 (3)
		N2B–C2B–N1B	106.2 (4)

Table 2 continued

Within the mineral moiety	Within the organic moiety	
	N2B–C2B–C1B	126.6 (4)
	N1B–C2B–C1B	127.2 (4)
	C4B–C3B–N1B	106.8 (4)
	C3B–C4B–N2B	106.4 (4)

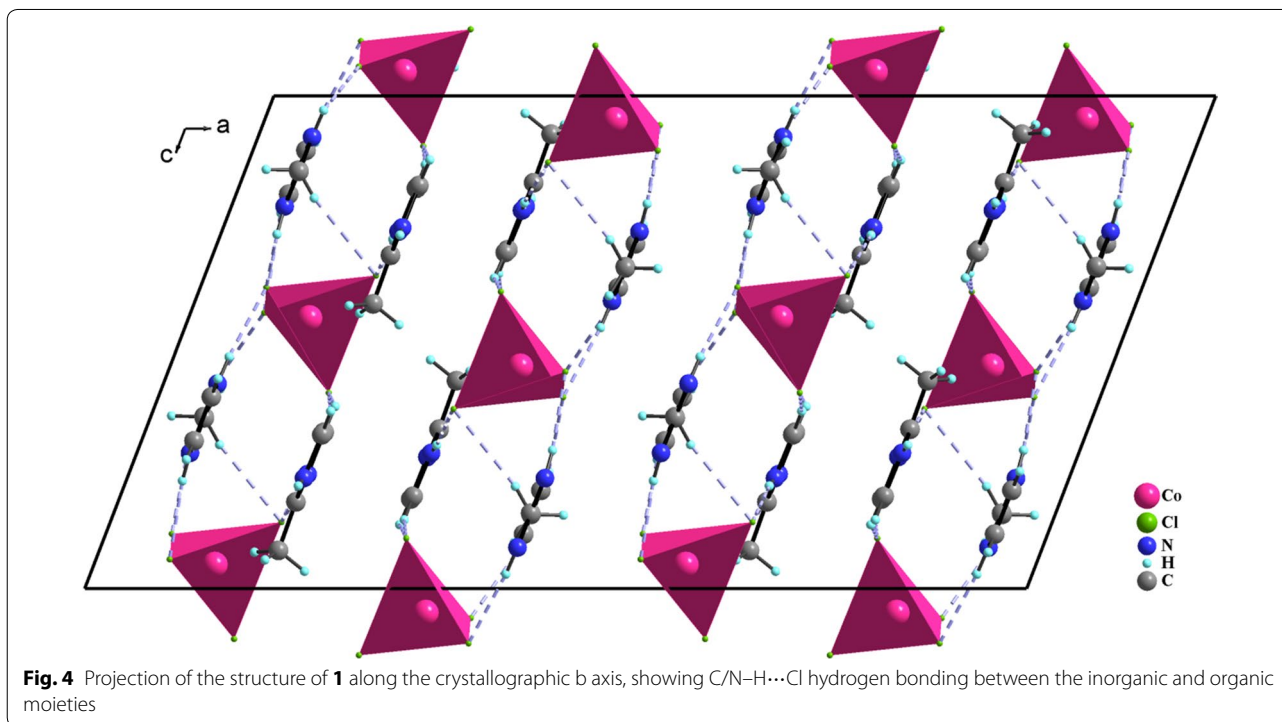
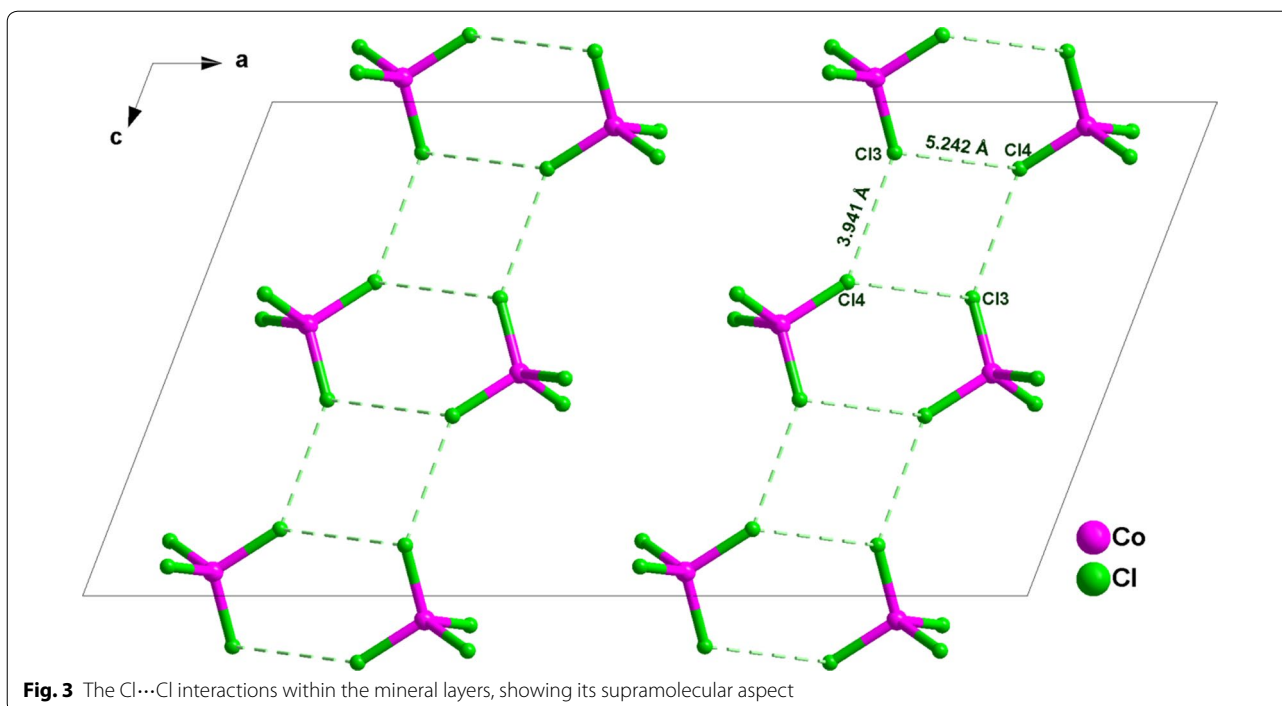
is no metallophilic Co...Co interaction in this compound as proposed by Das et al. [42]. One of the main cohesive forces responsible for molecular arrangements of halogen derivatives is the pattern of halogen...halogen intermolecular interactions. It is worth mentioning here, that in bis(2-methyl-1*H*-imidazolium)tetrachlorocobaltate(II) the shortest Cl...Cl contacts between copper sites related by unit cell translations along the *a* or *c* directions are 5.242 and 3.941 Å, respectively, thus proving the weak halogen interactions in these directions (Fig. 3).

As far as the cation is concerned, all the bond lengths and bond angles observed in aromatic rings of the 2-mim present no unusual features and are consistent with those observed in other homologous derivatives (Table 2) [40, 43]. The 2-methylimidazolium cation is essentially planar (maximum deviation from the mean plane through the imidazole ring is 0.0150 Å).

The packing of the structure can be regarded as alternating stacks of anions and layers of cations. The isolated molecules are involved in many intermolecular interactions leading to layers that are parallel to *bc* plane (Fig. 4). These layers are stabilized and governed significantly through extensive C/N–H...Cl hydrogen bonding between the inorganic and organic moieties and π ... π stacking interactions between the aromatic rings of the amine molecules themselves (Table 3). Indeed, the C...Cl distances vary from 3.422 (4) to 3.628 (4) Å, while the N...Cl distances vary from 3.160 (3) to 3.273 (3) Å. The centroid–centroid distance and dihedral angle between the aromatic rings are 3.62 Å and 0.00°, respectively, displaying typical π ... π stacking interactions (Fig. 5). These values are almost comparable to the corresponding values for intermolecular π ... π interactions, showing that π ... π contacts may further stabilize the structure. Then, both C/N–H...Cl and π ... π stacking interactions are the driving forces in generating a three-dimensional supramolecular network.

Thermal decomposition

The two compounds show similar thermal behavior, which further support their isomorphous structures. Thus, for simplicity the thermal properties of **1** only have been discussed. Thermogravimetric analyses of compound **1** were undertaken in the temperature range from 25 to 650 °C under flowing N₂ atmosphere with a heating



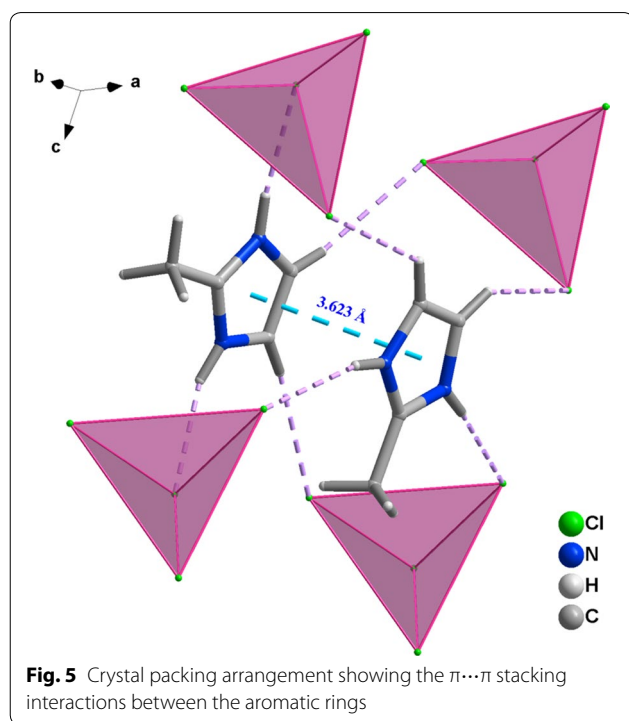
rate of 5 °C/min, leading to the simultaneous TGA/DTA profiles. The simultaneous (TG–DTA) curves and the three-dimensional representation of the powder diffraction patterns are shown in Figs. 6 and 7, respectively.

As shown in Fig. 6, the small mass gain observed at room temperature on the TG curve is explained by the strong hygroscopic character of the sample, as also observed when the sample is ground for XRPD analysis.

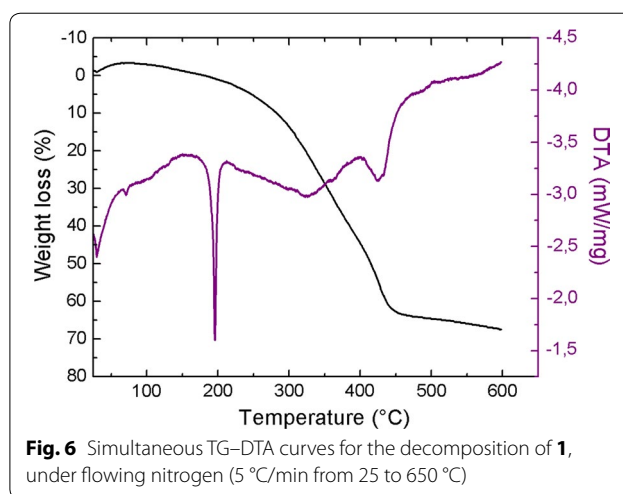
Table 3 Hydrogen-bonding geometry (Å, °) for 1 and 2

D-H...A	d (D-H) (Å)	d (H...A) (Å)	d (D...A) (Å)	∠ D-H...A (°)
(C₄H₇N₂)₂[CoCl₄] (1)				
N1A-H1A...Cl4	0.88	2.43	3.273 (3)	161
N2A-H2A...Cl4 ⁱ	0.88	2.51	3.213 (3)	174
N1B-H1B...Cl1	0.88	2.31	3.188 (3)	173
N2B-H2B...Cl2 ⁱⁱ	0.88	2.30	3.160 (3)	167
C2A-H2A1...Cl4	0.95	2.75	3.422 (4)	128
C3A-H3A...Cl4 ⁱ	0.95	2.75	3.532 (4)	141
C2B-H2B1...Cl1	0.95	2.69	3.576 (4)	155
C3B-H3B...Cl2 ⁱⁱ	0.95	2.71	3.628 (4)	163
(C₄H₇N₂)₂[ZnCl₄] (2)				
N1A-H1A...Cl4 ⁱ	0.88	2.34	3.222 (4)	176
N2A-H2A...Cl4	0.88	2.45	3.281 (4)	158
N1B-H1B...Cl1	0.88	2.30	3.158 (4)	164
N2B-H2B...Cl3 ⁱⁱ	0.88	2.32	3.199 (4)	173

Symmetry codes for 1: [(i) $x, y - 1, z$; (ii) $x, -y, z - 1/2$]; Symmetry codes for 2: [(i) $x, y + 1, z$; (ii) $x, -y - 1, z + 1/2$]



According to the TG curve, it is evident that compound **1** undergoes a single stage weight loss observed between 150 and 460 °C, accompanied by an intense endothermic peak at 195 °C and a shoulder endothermic peak at 425 °C, on the DTA thermogram. This mass loss corresponds to the elimination of the organic moiety and two



chloride atoms, (observed weight loss, 64.01%, theoretical, 64.57%). This decomposition process is confirmed by the three-dimensional representation of the powder diffraction patterns (Fig. 7). Indeed, the TDXD plot reveals that the precursor, (C₄H₇N₂)₂[CoCl₄], remains crystalline until 170 °C, while being subject to thermal expansion from room temperature, and then undergoes a complete structural destruction to become amorphous. The corresponding oxides, CoO and Co₃O₄, crystallize from 350 °C (ZnO for compound **2**).

Catalytic study

The transformation of a carbonyl group into an acetal is one of the most recurrent methods for protecting carbonyl groups in organic synthesis [44]. However, although this is an extensive explored approach, it still presents some inconveniences that should be overcome [45–56]. Therefore, the development of new catalytic structures to successfully perform this protection is of high interest for the progress of this field. Despite the number of reported works regarding this reaction, to the best of our knowledge the use of Co- [57, 58] and Zn-based catalysts [59, 60] has been less explored in the literature until now. In this spectrum of properties, we envisioned the possibility of testing the effectiveness of our metallic species in the acetalization reaction of aldehydes as a benchmark process.

In order to explore the efficiency of both candidates, we firstly tested their activity in the model acetalization reaction depicted in Table 4. Both catalytic structures shown the same order of reactivity at room temperature (compare entries 1–4 and 6–9). With a more concentrated reaction medium and 4 mol% of catalyst better yields are obtained (compare entries 2 and 4, and entries 7 and 8). At 40 °C catalyst **2** exhibited a slightly better reactivity

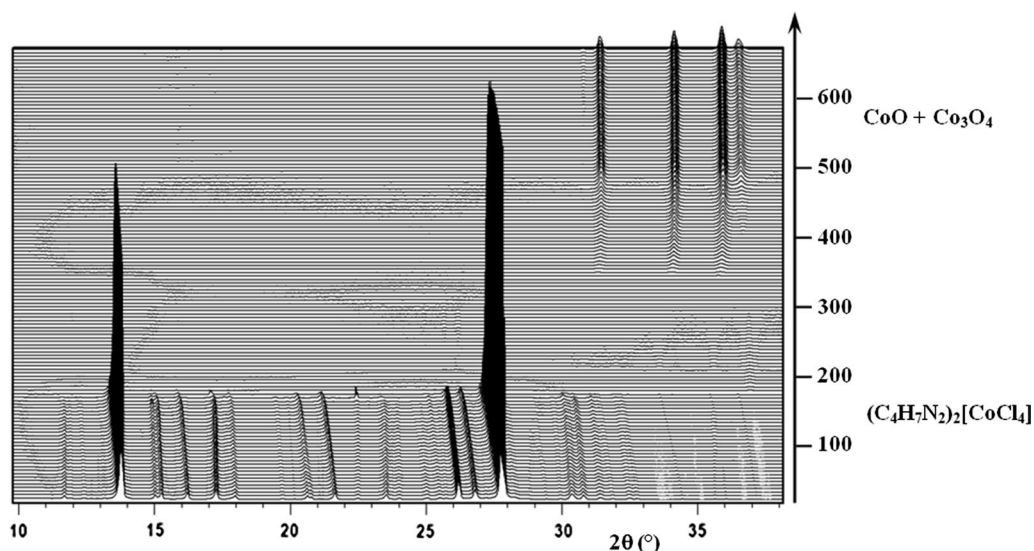
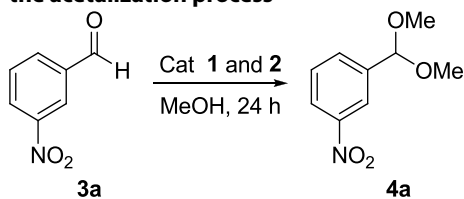


Fig. 7 TDXD plot for the decomposition of **1** in air ($7\text{ }^{\circ}\text{C h}^{-1}$ from 20 to $670\text{ }^{\circ}\text{C}$)

Table 4 Screening of the reaction conditions to optimize the acetalization process



Entry	Complex (mol%)	MeOH (mL)	Temperature ($^{\circ}\text{C}$)	Yield (%) ^a
1	1 (2)	0.25	r.t.	65
2	1 (4)	0.25	r.t.	78
3	1 (6)	0.25	r.t.	78
4	1 (4)	0.50	r.t.	59
5	1 (4)	0.25	40	92
6	2 (2)	0.25	r.t.	63
7	2 (4)	0.25	r.t.	83
8	2 (6)	0.25	r.t.	71
9	2 (4)	0.50	r.t.	67
10	2 (4)	0.25	40	97

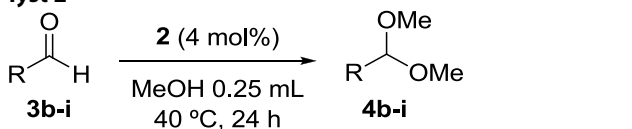
Otherwise indicated: a mixture of aldehyde **3a** (0.323 mmol) and catalysts **1** or **2** (4 mol%) in 0.25 mL MeOH, was stirred at $40\text{ }^{\circ}\text{C}$ for 24 h. After this time the reaction crudes were analysed by $^1\text{H NMR}$

^a Yields of **4a** [61] determined by $^1\text{H-NMR}$ spectroscopy

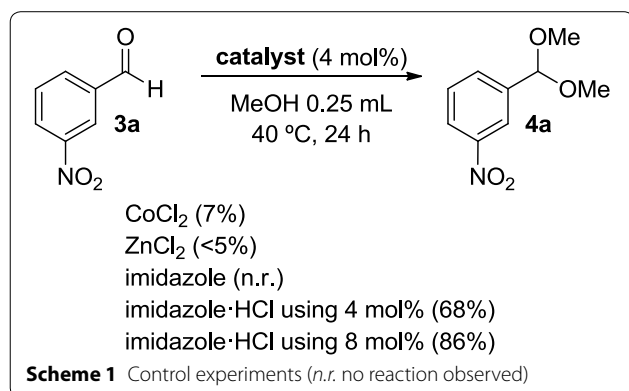
with an almost complete conversion of the process (compare entries 5 and 10). Although $\text{CH}(\text{OMe})_3$ is the commonly used source of acetalization in the protection of carbonyl compounds, interestingly, only MeOH is used in our protocol as the most accessible source.

After this screening, and with the best reaction conditions in hand, we extended our strategy to different substituted aldehydes as shown in Table 5. As reported in Table 5, the desired acetals **4b–i** were obtained with very good yields. The developed methodology was successfully applied to all aromatic aldehydes examined **3a–i** giving rise to really clean reaction crudes. Interestingly, neither inert atmosphere nor dry or other special conditions were needed to carry out the reactions. As a proof of fact, the reactions were performed in the absence of catalysts, demonstrating the efficiency of our catalytic species, since no reaction was observed in the background processes ($< 5\%$). It seems that the electronic effects over the aromatic ring affects to the reactivity of the process, since activated aldehydes, with electron-withdrawing groups in their structure, rendered better yields in comparison with non-activated ones (compare entries 1–5 with entries 6–8). Further catalytic studies are actually ongoing in our laboratory in order to explore additional reactions with both catalytic species.

In order to gain insight about the most active specie of our structures, we carried out some control experiments using the simplest species described in Scheme 1. In this sense, CoCl_2 and ZnCl_2 were used as direct precursors of the crystalline structures **1** and **2**, under the best reaction conditions above described in Table 5. Surprisingly, these metal species did not provide the acetalization reaction of aldehyde **3a**. Then, we focused on the contra ion of the crystal structures **1** and **2**, that is an imidazolium cation. First, imidazole was tested in the reaction as plausible catalyst but the reaction did not work as expected, since this process is acid promoted. In contrast,

Table 5 Scope of the acetalization reaction using catalyst 2


Entry	R	Product	Yield (%) ^a
1	4-ClPh, 3b	4b [62]	93
2	3-ClPh, 3c	4c [62]	81
3	4-BrPh, 3d	4d [62]	81
4	4-NO ₂ Ph, 3e	4e [62]	94
5	4-CNPh, 3f	4f [63]	94
6	4-PhPh, 3g	4g [64]	67
7	Ph, 3h	4h [62]	75
8	1-Naphthyl, 3i	4i [62]	70
9 ^b	3-NO ₂ Ph, 3a	4a	< 5

^a Yields determined by ¹H-NMR spectroscopy^b Reaction performed in the absence of catalyst

the generated chlorohydrate salt activated the reaction in a 68% as a weak acid catalyst. Since the crystal structures **1** and **2** bear two imidazolium molecules, the use of an 8 mol% of the acidic specie was also explored giving rise to an 86%. The activity observed with the imidazolium salt supports that the reactivity found with catalysts **1** and **2** is directly related with this salt species instead of the metal atom. This finding is also in agreement with the similar results observed when both species, **1** and **2**, were initially screened (Table 4). However, at this point we cannot discard a plausible synergic effect of the whole complex structure, since the results obtained with catalysts **1** and **2** are slightly better (Table 4, entries 5 and 10, respectively) than the results obtained just with imidazolium salt (Scheme 1). A possible acidification of the most acid proton in the imidazolium structure as a result of the interaction with the metal complex anion could be

tentatively suggested. Although more studies should be necessary to support the mechanism of this process using complexes **1** and **2**, a plausible catalytic cycle is proposed in Scheme 2 and the role of imidazolium salt, represented as H⁺, is depicted. The weak acid would be involved in the first step of the cycle activating the aldehyde to promote the addition of the first molecule of MeOH [65].

In-vitro antimicrobial activity

In this part and by way of comparison, we chose to study the antibacterial activity of the organic–inorganic hybrid metal(II) halides with 2-methylimidazole. Then the synthesized compounds as well as the copper complex based on 2-mim, recently published [34], were screened for their in vitro growth inhibiting activity against Gram-positive (*Enterococcus faecalis*, *Bacillus thuringiensis*, *Staphylococcus aureus*, *Micrococcus luteus* and *listeria*) and Gram-negative (*Salmonella typhimurium*, *Pseudomonas aeruginosa* and *Klebsiella pneumonia*) bacteria. The antibacterial activity was measured as the diameter of the clear zone of growth inhibition and the results were presented in Table 6. As can be seen in this table, (C₄H₇N₂)₂[CoCl₄] (**1**), (C₄H₇N₂)₂[ZnCl₄] (**2**) and (C₄H₇N₂)[CuCl₃(H₂O)] (**3**) possessed variable inhibition zones among the tested microorganisms ranging from 11 to 24 mm at the tested concentration (5 mg/mL). Cobalt complex was found to have a significant antibacterial activity against the Gram-negative bacteria tested compared to Gram-positive bacteria. In fact, compared to the ampicillin, (C₄H₇N₂)₂[CoCl₄] has the same diameter inhibition zones (24 mm) against *K. pneumoniae*. (C₄H₇N₂)₂[CoCl₄] exhibits a greater activity (20 mm) than the ampicillin against *S. Typhimurium*. According to the results presented in Table 6, (C₄H₇N₂)₂[ZnCl₄] was found to have a moderate activity against *E. faecalis*, *P. aeruginosa* and *S. Typhimurium*. No inhibition zones were observed for all the tested chemical compounds against *B. thuringiensis* and *M.l.* In fact, from these results can be deduced that these two Gram-positive bacteria were found to be very resistant. The antimicrobial results suggested that Co-complex exhibits higher biological activity against microbial tested strains in comparison to the ampicillin antibiotic.

Conclusions

Two new isostructural organic–inorganic hybrid materials, based on 2-methyl-1*H*-imidazole, **1** and **2**, were synthesized and fully structurally characterized. The basic unit structure of these compounds consists of one [M^{II}Cl₄]²⁻ ion and two crystallographically inequivalent 2-methylimidazolium cations. Furthermore, the analysis of their crystal packing reveals non-covalent interactions, including C/N–H⋯Cl hydrogen bonds and π⋯π

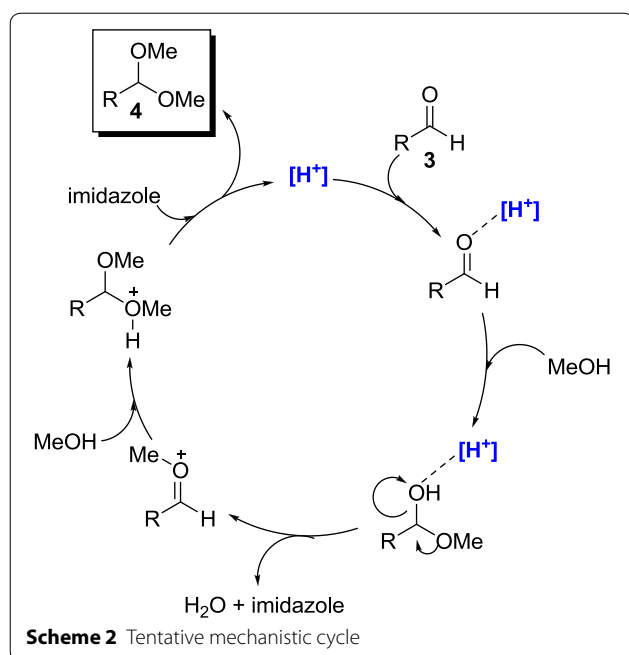


Table 6 Antibacterial activity of **1**, **2** and **3** against Gram (+) and Gram (–) bacteria strains

Bacteria strains	Inhibition zone diameter (mm)			
	1	2	3	Ampicillin
Gram +				
<i>S. aureus</i>	11 ± 0.5	nd	nd	40 ± 0.5
<i>E. faecalis</i>	13 ± 0.5	13 ± 0.5	nd	26 ± 0.5
<i>Listeria</i>	15 ± 0.5	nd	13 ± 0.5	33 ± 0.5
<i>B. thuringiensis</i>	nd	nd	nd	36 ± 0.5
<i>M. l</i>	nd	nd	nd	20 ± 0.5
Gram –				
<i>K. pneumoniae</i>	24 ± 0.5	nd	11 ± 0.5	24 ± 0.5
<i>P. aeruginosa</i>	13 ± 0.5	11 ± 0.5	nd	23 ± 0.5
<i>S. Typhimurium</i>	20 ± 0.5	12 ± 0.5	nd	15 ± 0.5

nd not detected

stacking interactions, to be the main factor governing the supramolecular assembly of the crystalline complexes. In view of the pivotal role of noncovalent interactions in the design of new materials, the theoretical calculation method of noncovalent interactions (NCI) is found to be an effective tool to understand the formation of these complex materials. The thermal decomposition of the complexes is a mono-stage process, confirmed by the three-dimensional representation of the powder diffraction patterns (TDXD). Additionally, we have demonstrated the efficiency of both metal complexes to act as catalysts in the acetalization reaction under very mild

conditions in the presence of MeOH, as the solvent of the reaction and as the unique source of acetalization. Moreover, the antimicrobial results suggested that metal-complexes exhibit significant antimicrobial activity. This study, in conjunction with the previous one [34], highlights again the structural and the biological diversities within the field of inorganic–organic hybrids.

Abbreviations

2mim: 2-methyl-1H-imidazole; DTA: differential thermal analysis; TGA: thermogravimetric analysis; IR: infrared; XRPD: X-ray powder diffraction.

Authors' contributions

All authors contributed to the discussion of the ideas which have resulted in the development of the strategy and descriptions of the methodology presented in this paper. AMBS performed the assays and prepared the manuscript. LBF was responsible for the antimicrobial activity assays. RPH conducted the catalytic studies. HN revised the manuscript. All authors read and approved the final manuscript.

Author details

¹ Laboratoire Physicochimie de l'Etat Solide, Département de Chimie, Faculté des Sciences de Sfax, Université de Sfax, BP 1171, 3000 Sfax, Tunisia. ² Unité Enzymes et Bioconversion, Ecole Nationale d'Ingénieurs de Sfax, PB 1173, 3038 Sfax, Tunisia. ³ Ecole Nationale Supérieure de Chimie de Rennes, 11 Allée de Beaulieu, 35708 Rennes cedex 7, France. ⁴ Laboratorio de Organocatálisis Asimétrica, Departamento de Química Orgánica, Instituto de Síntesis Química y Catálisis Homogénea (ISQCH), CSIC-Universidad de Zaragoza, C/Pedro Cerbuna 12, 50009 Saragossa, Spain.

Acknowledgements

The authors would like to thank gratefully the Faculty of Chemistry, University of Wrocław, Poland, for supplying single-crystal data collection. The authors are grateful, likewise, to Pr. Abdelmottaleb Ouederni for his assistance in TGA/DTA measurements of this study (The Unit of Joint Service of Recherche National School of Engineers of Gabes, University of Gabes, Tunisia). Ministerio de Economía, Industria y Competitividad MINECO-FEDER CTQ2017-88091-P is also acknowledged for financial support of our research.

Competing interests

The authors declare that they have no competing interests.

Availability of data and materials

Crystallographic data for CCDC-1433265 (**1**) and CCDC-1433266 (**2**) can be obtained free of charge from The Cambridge Crystallographic Data Centre via https://www.ccdc.cam.ac.uk/data_request/cif

Publisher's Note

Springer Nature remains neutral with regard to jurisdictional claims in published maps and institutional affiliations.

Received: 18 July 2017 Accepted: 15 February 2018

Published online: 01 March 2018

References

- Matulková I, Cihelka J, Pojarová M, Fejfarová K, Dušek M, Vaněk P, Kroupa J, Krupková R, Fábry J, Němec I (2012) A new series of 3,5-diamino-1,2,4-triazolium (1+) inorganic salts and their potential in crystal engineering of novel NLO materials. *CrystEngComm* 14:4625–4636
- Evans OR, Lin W (2001) Crystal engineering of nonlinear optical materials based on interpenetrated diamondoid coordination networks. *Chem Mater* 13:2705–2712

3. Zhang XM, Tong ML, Chen XM (2002) Hydroxylation of N-Heterocycle ligands observed in two unusual mixed-valence CuI/CuII complexes. *Angew Chem Int Ed* 41:1029
4. Lacroix PG, Malfant I, Bénard S, Yu P, Nakatani K (2001) Hybrid molecular-based magnets containing organic NLO chromophores: a search toward an interplay between magnetic and NLO behavior. *Chem Mater* 13:441
5. Clemente-León M, Coronado E, Martí-Gastaldo C, Romero FM (2011) Multifunctionality in hybrid magnetic materials based on bimetallic oxalate complexes. *Chem Soc Rev* 40:473
6. Fadhel H, Houcine N, Samia Y, Turnbull MM, Tahar M, Thierry B (2011) Synthesis, characterization and magnetic properties of four new organically templated metal sulfates [C₅H₁₄N₂][MII(H₂O)₆](SO₄)₂, (MII = Mn, Fe Co, Ni). *Dalton Trans* 40:11613
7. Matulková I, Cihelka J, Fejfarová K, Dušek M, Pojarová M, Vaněk P, Kroupa J, Šala M, Krupková R, Němec I (2011) Semi-organic salts of aniline with inorganic acids: prospective materials for the second harmonic generation. *CrystEngComm* 13:4131
8. Clemente-León M, Coronado E, Galán-Mascarós JR, Gómez-García CJ, Canadell E (2000) Hybrid molecular materials based upon the photochromic nitroprusside complex, [Fe(CN)₅NO]²⁻, and organic π -Electron donors. synthesis, structure, and properties of the radical salt (TTF)₇[Fe(CN)₅NO]₂ (TTF = Tetrathiafulvalene). *Inorg Chem* 39:5394
9. Coronado E, Galán-Mascarós J, Gómez-García CJ, Laukhin V (2000) Coexistence of ferromagnetism and metallic conductivity in a molecule-based layered compound. *Nature* 408:447
10. Yaghi OM, O'Keeffe M, Ockwig NW, Chae HK, Eddaoudi M, Kim J (2003) Reticular synthesis and the design of new materials. *Nature* 423:705
11. Houcine N, Fadhel H, Tahar M, Mac Leod TCO, Kopylovich MN, Kamran MT, Pombeiro AJL (2013) 2-Dihydropiperazine-M^{II} (M^{II} = Cu^{II}, Fe^{II}, Co^{II}, Zn^{II}) double sulfates and their catalytic activity in diastereoselective nitroaldol (Henry) reaction. *Dalton Trans* 42:399
12. Erer H, Yeşilel OZ, Darcan C, Büyükgüngör O (2009) Synthesis, spectroscopic, thermal studies, antimicrobial activities and crystal structures of Co (II), Ni (II), Cu (II) and Zn (II)-orotate complexes with 2-methylimidazole. *Polyhedron* 28:3087
13. Alvarado E, Badaj AC, Larocque TG, Chem Lavoie G G (2012) N-Heterocyclic carbenes and imidazole-2-thiones as ligands for the gold(I)-catalysed hydroamination of phenylacetylene. *Eur J* 18:12112
14. Burling S, Field LD, Messerle BA, Rumble SL (2007) Late transition metal catalyzed intramolecular hydroamination: the effect of ligand and substrate structure. *Organometallics* 26:4335
15. Burling S, Field LD, Messerle BA, Turner P (2004) Intramolecular hydroamination catalyzed by cationic rhodium and iridium complexes with bidentate nitrogen-donor ligands. *Organometallics* 23:1714
16. Burling S, Field LD, Messerle BA (2000) Hydroamination of alkynes catalyzed by a cationic rhodium (I) complex. *Organometallics* 19:87
17. Elgafi S, Field LD, Messerle BA, Turner P, Hambley TW (1999) Rhodium complexes containing bidentate imidazolyl ligands: synthesis and structure. *J Organomet Chem* 588:69
18. Elgafi S, Field LD, Messerle BA, Hambley TW, Turner P (1997) Synthesis of novel ruthenium complexes containing bidentateimidazole-based ligands. *J Chem Soc Dalton Trans* 13:2341
19. Done MC, Rüther T, Cavell KJ, Kilner M, Peacock EJ, Braussaud N, Skelton BW, White A (2000) Novel cationic and neutral Pd(II) complexes bearing imidazole based chelate ligands: synthesis, structural characterisation and catalytic behaviour. *J Organomet Chem* 607:78
20. Liu YM, Lin YC, Chen WC, Cheng JH, Chen YL, Yap GPA, Sun SS, Ong TG (2012) Synthesis and characterization of para-pyridine linked NHC palladium complexes and their studies for the Heck-Mizoroki coupling reaction. *Dalton Trans* 41:7382–7389
21. Huynh HV, Jothibasu R (2011) Syntheses and catalytic activities of Pd(II) dicarbene and hetero-dicarbene complexes. *J Organomet Chem* 696:3369
22. Yang WH, Lee CS, Pal S, Chen YN, Hwang WS, Lin IJB, Wang JC (2008) Novel Ag(I), Pd(II), Ni(II) complexes of N, N'-bis-(2,2-diethoxyethyl) imidazole-2-ylidene: synthesis, structures, and their catalytic activity towards Heck reaction. *J Organomet Chem* 693:3729
23. Rüther T, Done MC, Cavell KJ, Peacock EJ, Skelton BW, White AH (2001) Novel methylpalladium (II) complexes bearing tridentate imidazole-based chelate ligands: synthesis, structural characterization and reactivity. *Organometallics* 20:5522
24. Omar K, Walid R, Thierry B, Kamran TM, Kopylovich MN, Houcine N (2013) Inorganic-organic hybrid double sulfates as catalysts of the diastereoselective nitroaldol reaction. *J Organomet Chem* 136:741–742
25. Cheruzel LE, Cecil MR, Edison SE, Mashuta MS, Baldwin MJ, Buchanan RM (2006) Structural and spectroscopic characterization of copper(II) complexes of a new bisamide functionalized imidazole tripod and evidence for the formation of a mononuclear end-on Cu–OOH species. *Inorg Chem* 45:319
26. Wallar BJ, Lipscomb JD (1996) Dioxygen activation by enzymes containing binuclear non-heme iron clusters. *Chem Rev* 96:2625
27. Flint DH, Allen RM (1996) Iron–sulfur proteins with nonredox functions. *Chem Rev* 96:2315
28. Holm RH, Kennepohl P, Solomon EI (1996) Structural and functional aspects of metal sites in biology. *Chem Rev* 96:2239
29. Breslow R, Hunt JT, Smiley R, Tarnowski T (1983) Synthesis of some poly-imidazole ligands related to zinc enzymes. *J Am Chem Soc* 105:5337
30. Siddiqi ZA, Khalid M, Kumar S, Shahid M, Noor S (2010) Antimicrobial and SOD Activities of novel transition metal complexes of pyridine-2,6-dicarboxylic acid containing 4-picoline as auxiliary ligand. *Eur J Med Chem* 45:264–269
31. Delaney S, Pascaly M, Bhattacharya PK, Han K, Barton JK (2002) Oxidative damage by ruthenium complexes containing the dipyrrophenazine ligand or its derivatives: a focus on intercalation. *Inorg Chem* 41:1966–1974
32. Serbest K, Colak A, Güner S, Karaböcek S, Kor-mali F (2001) Copper(II)-manganese(II) complexes of 3,3'-(1,3-propanediyl)diimine)bis-(3-methyl-2-butanone)dioxime with superoxide dismutase-like activity. *Transit Met Chem* 26:625–629
33. Vogel AI (1989) *Textbook of practical organic chemistry*, 5th edn. Longman, London
34. Assila MBS, Houcine N, Miroslaw A, Magdalena F (2016) 0D and 1D copper(II) coordination polymers based on 2-methyl-1Himidazole: structural, vibrational and magnetic characterizations. *J Organomet Chem* 805:42
35. CrysAlis CCD and CrysAlis RED (2010) Xcalibur R software. Oxford Diffraction Ltd, Abingdon
36. Farrugia LJ (1999) WinGX suite for small molecule single crystal crystallography. *J Appl Crystallogr* 32:837
37. Sheldrick GM (2008) A short history of SHELX. *Acta Cryst A* 64:112
38. Brandenburg K (2012) DIAMOND. Version 3.2i. Crystal Impact GbR, Bonn
39. Harbone JB, Dey PM (1991) *Methods in plant biochemistry*, vol 6. Academic Press, London, p 47
40. Hachula B, Nowak M, Kusz J (2010) Crystal and molecular structure analysis of 2-methylimidazole. *J Chem Crystallogr* 40(3):201
41. Naumov P, Ristova M, Šoptrajanov B, Zugik M (2001) Vibrational spectra of bis(acetato)tetrakis(imidazole)copper(II). *J Mol Struct* 598:235
42. Das S, Hung CH, Goswami S (2003) Blue dimetallic complexes of two heavy metal ions Cd^{II} and Hg^{II} with an extended nitrogen donor ligand. preparation, spectral characterization, and crystallographic studies. *Inorg Chem* 42:8592
43. Hachula B, Pedras M, Pentak D, Nowak M, Kusz J, Borek J (2009) Effect of an industrial chemical waste on the uptake. *Acta Crystallogr C* 65:215
44. Greene TW, Wuts PGM (1999) *Protective groups in organic synthesis*, 3rd edn. Wiley, New York
45. Karimi B, Golshani B (2002) Iodine-catalyzed, efficient and mild procedure for highly chemoselective acetalization of carbonyl compounds under neutral aprotic conditions. *Synthesis* 784–788. <https://doi.org/10.1055/s-2002-25775>
46. Gopinath R, Haque SJ, Patel BK (2002) Tetrabutylammonium tribromide (TBATB) as an efficient generator of HBr for an efficient chemoselective reagent for acetalization of carbonyl compounds. *J Org Chem* 67:5842
47. Lee SH, Lee JH, Yoon CM (2002) An efficient protection of carbonyls and deprotection of acetals using decaborane. *Tetrahedron Lett* 43:2699
48. Leonard NM, Oswald MC, Freiberg DA, Nattier BA, Smith RC, Mohan RS (2002) A simple and versatile method for the synthesis of acetals from aldehydes and ketones using bismuth triflate. *J Org Chem* 67:5202
49. Patel SM, Chudasama UV, Ganesphure PA (2003) Ketalization of ketones with diols catalyzed by metal(IV) phosphates as solid acid catalysts. *J Mol Catal A Chem* 194:267
50. Chen CT, Weng SS, Kao JQ, Lin CC, Jan MD (2005) Stripping off water at ambient temperature: direct atom-efficient acetal formation between

- aldehydes and diols catalyzed by water-tolerant and recoverable vanadyl triflate. *Org Lett* 7:3343
51. Kumar R, Chakraborti AK (2006) Copper(II) tetrafluoroborate as a novel and highly efficient catalyst for acetal formation. *Tetrahedron Lett* 46:8319
 52. Smith BM, Graham AE (2006) Indium triflate mediated acetalization of aldehydes and ketones. *Tetrahedron Lett* 47:9317
 53. Williams DBG, Lawton MG (2008) Highly atom efficient aluminium triflate catalysed acetal formation. *Green Chem* 10:914
 54. Gregg BT, Golden KC, Quinn JF (2008) Indium(III)trifluoromethanesulfonate as a mild, efficient catalyst for the formation of acetals and ketals in the presence of acid sensitive functional groups. *Tetrahedron* 64:3287
 55. Miao Z, Xu L, Song H, Zhao H, Chou L (2013) One-pot synthesis of ordered mesoporous zirconium oxophosphate with high thermostability and acidic properties. *Catal Sci Technol* 3:1942
 56. Zhao S, Jia Y, Song YF (2014) Acetalization of aldehydes and ketones over $H_4[SiW_{12}O_{40}]$ and $H_4[SiW_{12}O_{40}]/SiO_2$. *Catal Sci Technol* 4:2618
 57. Velusamy S, Punniyamurthy T (2004) Cobalt(II)-catalyzed chemoselective synthesis of acetals from aldehydes. *Tetrahedron Lett* 45:4917
 58. Rajabi FJ (2010) Cobalt (II) schiff base functionalized mesoporous silica as an efficient and recyclable chemoselective acetalization catalyst. *Iran Chem Soc* 7:695
 59. Roy A, Rahman M, Das S, Kundu D, Kundu SK, Majee A, Hajra A (2009) Zinc chloride as an efficient catalyst for chemoselective dimethyl acetalization. *Synth Commun* 39:590
 60. Salem S, Houcine N, Thierry B, Raquel PH (2016) Crystallisation, thermal analysis and acetal protection activity of new layered Zn(II) hybrid polymorphs. *CrystEngComm* 18:5365
 61. Dear AE, Liu HB, Mayes PA, Perlmutter P (2006) Conformational analogues of Oxamflatin as histone deacetylase inhibitors. *Org Biomol Chem* 4:3778
 62. Ito S, Hayashi A, Komai H, Yamaguchi H, Kubota Y, Asami M (2011) Mesoporous aluminosilicate-catalyzed allylation of carbonyl compounds and acetals. *Tetrahedron* 67:2081
 63. Langhals H, Becherer T, Lindner J, Obermeier A (2007) The fluorescence labelling of primary amines with perylenetetracarboxydiimides. *Eur J Org Chem*, p 4328
 64. Barba I, Chinchilla R, Gomez C (1990) Synthesis of phenyl substituted cyclohexa-1,4-dienes and cyclohexa-2,5-dienones by anodic methoxylation of alkylbiphenyls. *Tetrahedron* 46:7813
 65. Barbara P, Stephen JC (2008) Unexpected catalysis: aprotic pyridinium ions as active and recyclable Brønsted acid catalysts in protic media. *Org Lett* 10:4935

Submit your manuscript to a SpringerOpen[®] journal and benefit from:

- Convenient online submission
- Rigorous peer review
- Open access: articles freely available online
- High visibility within the field
- Retaining the copyright to your article

Submit your next manuscript at ► springeropen.com
